Nonresonant pump/probe electronic Raman scattering within nonequilibrium dynamical mean-field theory

J. K. Freericks, O. P. Matveev, A. M. Shvaika, T. P. Devereaux

J. K. Freericks, O. P. Matveev, A. M. Shvaika, T. P. Devereaux, "Nonresonant pump/probe electronic Raman scattering within nonequilibrium dynamical mean-field theory," Proc. SPIE 10638, Ultrafast Bandgap Photonics III, 1063807 (8 May 2018); doi: 10.1117/12.2305103

SPIE.

Event: SPIE Defense + Security, 2018, Orlando, Florida, United States

Invited Paper

Nonresonant pump-probe electronic Raman scattering within nonequilibrium dynamical mean-field theory

J. K. Freericks[a], O. P. Matveev[b], A. M. Shvaika[b], and T. P. Devereaux[c,d]

[a]Department of Physics, Georgetown University, 37th and O Sts. NW, Washington, DC 20057, USA

[b]Institute for Condensed Matter Physics of the National Academy of Sciences of Ukraine, 1 Svientsitskii St., Lviv, 79011, Ukraine

[c]Geballe Laboratory for Advanced Materials, 476 Lomita Mall, Stanford University, Stanford, CA 94305, USA

[d]Stanford Institute for Materials and Energy Sciences, SLAC National Accelerator Laboratory, 2575 Sand Hill Rd., Menlo Park, CA 94025, USA

ABSTRACT

We develop the theory for nonresonant Raman scattering of strongly correlated electrons in time-resolved pump-probe experiments. The electrons are initially pumped with an intense pulse of light and then a probe pulse measures the Raman response function after an adjustable time delay. We describe how the width of the probe pulse and the strength of the electron correlations affect the Raman cross section. The theory is developed for the case of B_{1g} symmetry, where incident and scattered light are polarized perpendicular to each other. We illustrate the exact solution with the Falicov-Kimball model, which is solved via nonequilibrium dynamical mean-field theory.

Keywords: Nonequilibrium Raman scattering, Nonequilibrium dynamical mean-field theory, Pump-probe spectroscopy, Strongly correlated electrons, Falicov-Kimball model

1. INTRODUCTION

Recently, there have been numerous pump-probe experiments, where an intense and ultrafast laser pump drives an electronic system into a far from equilibrium state and then weaker probe pulses are applied to study the system as it relaxes back to equilibrium.[1–4] Our interest is in developing theory for a wide range of different pump-probe experiments performed on strongly correlated materials. Here, we focus on nonresonant electronic Raman scattering. The Raman scattering cross section is an important probe of such materials because it provides symmetry selective information about two-particle electronic excitations in the solid. While a theoretical description of the electronic Raman shift is well developed for strongly correlated materials in equilibrium,[5–9] including the nonresonant, mixed, and resonant processes, there is no theory for Raman scattering in nonequilibrium. Recent pump-probe Raman scattering experiments on the phonons in graphite[10] reveal a novel electron-phonon relaxation pathway. That work encouraged us to develop the theory for pump-probe electronic Raman scattering.

We use the Falicov-Kimball model in our analysis because it is the simplest model of electron correlations[11] and it has an exact solution within dynamical mean-field theory (DMFT)[12] (for a review see Ref. 13). The many-body formalism for nonequilibrium DMFT is developed within the Kadanoff-Baym-Keldysh approach.[14,15] Details for how one solves nonequilibrium DMFT for the uniform phase of the Falicov-Kimball model have already appeared.[16] Here we generalize this theory to Raman scattering.

Send correspondence to J.K. Freericks
E-mail: James.Freericks@georgetown.edu, Telephone: +1 202 687 6159

Ultrafast Bandgap Photonics III, edited by Michael K. Rafailov, Proc. of SPIE Vol. 10638, 1063807 · © 2018 SPIE · CCC code: 0277-786X/18/$18 · doi: 10.1117/12.2305103

2. FORMALISM

In nonequilibrium, the Hamiltonian explicitly depends on time. For concreteness, we examine the so-called Falicov-Kimball model, which contains itinerant and localized electrons that mutually interact. The Hamiltonian of this model is equal to:

$$\mathcal{H} = \sum_i \{U n_{ic} n_{if} - \mu n_{ic} + E_f n_{if}\} - \sum_{ij} t_{ij}(t) c_i^\dagger c_j, \tag{1}$$

where $n_{ic} = c_i^\dagger c_i$ and $n_{if} = f_i^\dagger f_i$ are the number operators of the itinerant (c) and localized (f) electrons, respectively. The local term describes the Coulomb interaction between the localized and itinerant electrons on the ith site, the chemical potential μ of the c-electrons, and the site-energy E_f of the f-electrons. The nonlocal kinetic-energy term of the Hamiltonian describes hopping of itinerant electrons between the nearest-neighbor sites. The time-dependent hopping term describes the spatially uniform and time-varying electric pump via the Peierls' substitution. The vector potential enters into the hopping as follows:

$$t_{i,j}(t) = t_{i,j} e^{-i \int_{\mathbf{R}_i}^{\mathbf{R}_j} dr \mathbf{A}(r,t)}, \tag{2}$$

with $\mathbf{R}_i$ the position vector for the ith lattice site. We ignore all magnetic field and relativistic effects in the pump field, which violates Maxwell's equation, but the violations should be small because the electric field dominates the response. We work with a vector potential in the Hamiltonian gauge $\mathbf{E}(t) = -d\mathbf{A}(t)/dt$. To model a pump-probe experiment, where the electromagnetic energy is delivered to material with a laser pulse, we choose the pump field to be sinusoidally varying with a Gaussian envelope of the form

$$\mathbf{E}(t) = \mathbf{E}_0 \cos(\omega_p (t - t_p)) e^{-\frac{(t-t_p)^2}{\sigma_p^2}}, \tag{3}$$

where $\mathbf{E}_0$ is the magnitude of the field at time $t = t_p$ (the maximum of the pump pulse), and ω_p and σ_p define the frequency and width of the envelope of the pump pulse, respectively. We work in units where $\hbar = c = e = a = 1$.

In order to describe the time evolution of the system, we start the system in equilibrium at an initial temperature $T = 1/\beta$, which is described by the density matrix $\exp(-\beta \mathcal{H}(t \to -\infty)/\mathcal{Z}$, where $\mathcal{Z} = \mathrm{Tr} \exp[-\beta \mathcal{H}(t \to -\infty)]$ is the partition function. The system is evolved forward in time with the evolution operator (time-ordered product) $U(t_2, t_1) = \mathcal{T}_t \exp\left[-i \int_{t_1}^{t_2} d\tilde{t} \mathcal{H}(\tilde{t})\right]$ so that the state at time t, which was initially in an eigenstate $|n\rangle$ of the Hamiltonian $\mathcal{H}(t \to -\infty)$, becomes

$$|n(t)\rangle = U(t, -\infty)|n\rangle = \mathcal{T}_t \exp\left\{-i \int_{-\infty}^{t} d\tilde{t} \mathcal{H}(\tilde{t})\right\} |n\rangle. \tag{4}$$

The pump-probe experiment involves two pulses (the pump and the probe), so vector potential in Eq. (2) has two terms $\mathbf{A}(t) = \mathbf{A}_{\mathrm{pump}}(t) + \mathbf{A}_{\mathrm{probe}}(t)$. The pump field $\mathbf{A}_{\mathrm{pump}}(t)$ is large and is treated nonpertubatively, while probe field $\mathbf{A}_{\mathrm{probe}}(t)$ is weak and its effect is expanded perturbatively. Raman scattering is a second order process, so the nonresonant vertex includes two factors of the probe field. We analyze the problem by summing the quantum states which include the Raman vertex acting at any time between the start and the end of the experiment. The state evolves as follows:

$$|n(t \to \infty)\rangle = \frac{1}{2} \int_{-\infty}^{\infty} d\tilde{t}\, U(\infty, \tilde{t}) \mathbf{A}^\alpha_{\mathrm{probe}}(\tilde{t}) \gamma_{\alpha\beta}(\tilde{t}) \mathbf{A}^\beta_{\mathrm{probe}}(\tilde{t}) U(\tilde{t}, -\infty)|n\rangle, \tag{5}$$

where $U(t_2, t_1)$ is the evolution operator with just the pump field (the repeated indices α and β are summed over). The factor $1/2$ arises from the coupling strength, given by $e^2/(2\hbar^2 c^2) = 1/2$ in our units. The stress tensor operator $\gamma_{\alpha\beta}(t)$ is defined in the momentum representation by

$$\gamma_{\alpha\beta}(t) = \sum_{\mathbf{k}} \frac{d^2 \epsilon(\mathbf{k}, t)}{dk_\alpha dk_\beta} c_{\mathbf{k}}^\dagger c_{\mathbf{k}}, \quad \text{and} \quad \epsilon(\mathbf{k}, t) = -\frac{t^*}{\sqrt{D}} \sum_{\alpha=1}^{D} \cos(k_\alpha - A^\alpha_{\mathrm{pump}}(t)). \tag{6}$$

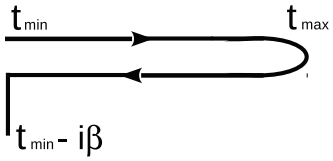

Figure 1. Kadanoff-Baym-Keldysh contour, which runs from time $t_{\min}$ to time $t_{\max}$ and back and then along the imaginary axis to $t_{\min} - i\beta$.

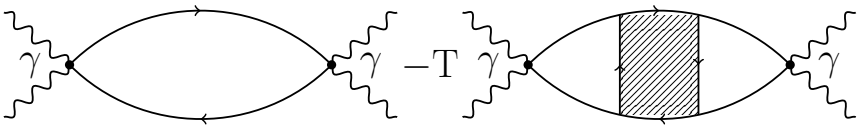

Figure 2. Diagrammatic series for the nonresonant Raman scattering probability.

The standard second quantization representation of the probe field operator describes the creation and annihilation of photons with frequency ω and polarization $\mathbf{e}$ as follows:

$$A^{\alpha}_{\text{probe}}(t) = s(t)e_{\alpha}(e^{i\omega t}a^{\dagger} + e^{-i\omega t}a), \quad \text{and} \quad s(t) = \frac{1}{\sigma_b\sqrt{\pi}}e^{-\frac{(t-t_0)^2}{\sigma_b^2}}, \tag{7}$$

where probe pulse envelope function $s(t)$ is a Gaussian of width σ_b, which determines the resolution of the Raman scattering—the larger σ_b the higher the energy resolution and the lower the time resolution and *vice versa*. Below we put $t_p = 0$ and the time t_0 is the time delay of the probe pulse with respect to the pump pulse.

Next, we develop formalism proposed by Nozières and Abrahams[17] to calculate the probability of Raman scattering for the pumped system. The scattering amplitude is equal to the weighted sum of the mod square of the final states in Eq. (5) weighted by the thermal factors and summed over all states. The total probability of the Raman transition is defined by:

$$R_{\gamma\gamma} = \sum_n \frac{e^{-\beta E_n}}{\mathcal{Z}}\langle n(t\to\infty)|n(t\to\infty)\rangle. \tag{8}$$

The probe functions that are in the probe vector potentials determine the time when the Raman scattering occurs. In most experiments, we actually measure the probability as a function of the changed light frequency. In this case, Nozières and Abrahams[17] showed that we need to compute the countour-ordered two-particle Green's function, which is built on two stress tensor operators

$$R^{c}_{\gamma\gamma}(t,t') = -i\text{Tr}\frac{e^{-\beta\mathcal{H}(t\to-\infty)}}{\mathcal{Z}}\mathcal{T}_c\gamma(t)\gamma(t') \tag{9}$$

with times t and t' belonging to the Kadanoff-Baym-Keldysh contour[14,15] in Fig. 1. We must place the times t and t' on the different branches of the contour with t farther advanced than t'. This corresponds to definition of the greater Green's function $R^{>}_{\gamma\gamma}(t,t') = -i\text{Tr}\exp(-\beta\mathcal{H}(t\to-\infty))\gamma(t)\gamma(t')/\mathcal{Z}$. The diagrammatic series is plotted in Fig. 2 and it consists of two terms: the bare and renormalized bubbles. The bubbles are constructed from the greater $G^{>}(t,t') = -i\text{Tr}\exp(-\beta\mathcal{H}(t\to-\infty))c(t)c^{\dagger}(t')/\mathcal{Z}$ and the lesser $G^{<}(t,t') = i\text{Tr}\exp(-\beta\mathcal{H}(t\to-\infty))c(t)c^{\dagger}(t')/\mathcal{Z}$ single-particle Green's functions, also defined on the contour in Fig. 1. Every apex in Fig. 2 brings a stress tensor factor, which contains the product of two polarization vectors. These are defined by the symmetry of experiment and in this paper, we restrict ourselves to the B_{1g} symmetry only. In this case, the polarizations of incident and scattered light are equal to $\mathbf{e}^i = (1,1,1,...)$ and $\mathbf{e}^f = (-1,1,-1,...)$ and the appropriate expression for stress tensor factor becomes

$$\bar{\gamma}_{B_{1g}}(\mathbf{k},t) = \frac{t^*}{\sqrt{D}}\sum_{\alpha=1}^{D}(-1)^{\alpha}\cos\left(k_{\alpha} - A^{\alpha}_{\text{pump}}(t)\right). \tag{10}$$

In DMFT an irreducible charge vertex is local and when we calculate the renormalized bubble, the summation over momenta in Fig. 2 is applied to the product of two Green's function and one factor of $\bar{\gamma}_{B_{1g}}(\mathbf{k},t)$. Because the result is the same in each spatial direction when the field is applied along the diagonal direction, the sum vanishes due to the $(-1)^\alpha$ factor, just like in equilibrium:[8]

$$\frac{t^*}{\sqrt{D}}\sum_{\mathbf{k}}\sum_{\alpha=1}^{D}(-1)^\alpha\cos\left(k_\alpha - A^\alpha_{\rm pump}(t)\right)G^{>}_{\mathbf{k}}(t,t')G^{<}_{\mathbf{k}}(t',t)=0, \tag{11}$$

note that this cancellation of vertex corrections does not arise due to a parity argument (which fails in nonequilibrium), but from isotropy (which survives in nonequilibrium). Hence, we end up with a bare bubble which includes the product of two Green's functions and two stress tensor factors $\bar{\gamma}_{B_{1g}}(\mathbf{k},t)\bar{\gamma}_{B_{1g}}(\mathbf{k},t')$. To sum over momenta $\mathbf{k}$, we switch to an integration over energy with a Gaussian density of states $\rho(\epsilon)=\exp(-\epsilon^2/t^{*2})/\sqrt{\pi}$, which results in the following expression for the bare bubble:

$$\begin{aligned}&\frac{t^{*2}}{D}\sum_{\mathbf{k}}\sum_{\alpha=1}^{D}\cos\left(k_\alpha - A^\alpha_{\rm pump}(t)\right)\cos\left(k_\alpha - A^\alpha_{\rm pump}(t')\right)G^{>}_{\mathbf{k}}(t,t')G^{<}_{\mathbf{k}}(t',t)\\ &=\frac{t^{*2}}{2}\cos\left(A_{\rm pump}(t)-A_{\rm pump}(t')\right)\int d\epsilon\int d\bar{\epsilon}\rho(\epsilon)\rho(\bar{\epsilon})G^{>}_{\epsilon,\bar{\epsilon}}(t,t')G^{<}_{\epsilon,\bar{\epsilon}}(t',t),\end{aligned} \tag{12}$$

where $\bar{\epsilon}=\bar{\epsilon}(\mathbf{k},t)=-t^*\sum_{\alpha=1}^{D}\sin\left(k_\alpha - A^\alpha_{\rm pump}(t)\right)/\sqrt{D}$. We have assumed a field applied in the diagonal direction so that $A^\alpha = A$ is independent of the spatial direction. Finally, one needs to average the Raman scattering probability over the photon states with appropriate envelope functions $s(t)$ from Eq. (7) and then perform the Fourier transform from the time representation to the frequency representation. We determine the final expression for the nonresonant Raman scattering cross-section in the B_{1g} channel to be

$$R^N_{B_{1g}}(\Omega,t_0)=\frac{t^{*2}}{2}\int dt\int dt' s^2(t)s^2(t')e^{i\Omega(t-t')}\cos\left(A_{\rm pump}(t)-A_{\rm pump}(t')\right)\int d\epsilon\int d\bar{\epsilon}\rho(\epsilon)\rho(\bar{\epsilon})G^{>}_{\epsilon,\bar{\epsilon}}(t,t')G^{<}_{\epsilon,\bar{\epsilon}}(t',t), \tag{13}$$

where Ω is frequency shift during scattering. Since each probe field operator in Eq. (8) has an envelope function $s(t)$, it arises squared in the final formula above (the probe pulses are centered at t_0). This suppresses the Raman signal significantly compared to what is observed in equilibrium.

In addition to the cross-section, we can examine the Raman response function. In equilibrium, the Raman cross-section is defined straightforwardly from the response function, which corresponds to the retarded Raman Green's function (which also defines the density of states). In nonequillibrium, the response function can be defined either from the difference of the Stokes and anti-Stokes contributions to the Raman scattering cross-section

$$\chi^{as}_N(\Omega,t_0)=R^N_{B_{1g}}(\Omega,t_0)-R^N_{B_{1g}}(-\Omega,t_0), \tag{14}$$

which gives an antisymmetric response function by its definition, or directly from the retarded Green's function

$$\begin{aligned}R^r(t,t') &= \frac{1}{2}\left[R^{<}(t,t')-R^{>}(t,t')+R^{t}(t,t')-R^{\bar{t}}(t,t')\right]=\frac{t^{*2}}{2}\cos\left(A_{\rm pump}(t)-A_{\rm pump}(t')\right)\int d\epsilon\int d\bar{\epsilon}\rho(\epsilon,\bar{\epsilon})\\ &\times\frac{1}{2}\left[G^{<}_{\epsilon,\bar{\epsilon}}(t,t')G^{>}_{\epsilon,\bar{\epsilon}}(t',t)-G^{>}_{\epsilon,\bar{\epsilon}}(t,t')G^{<}_{\epsilon,\bar{\epsilon}}(t',t)+G^{t}_{\epsilon,\bar{\epsilon}}(t,t')G^{t}_{\epsilon,\bar{\epsilon}}(t',t)-G^{\bar{t}}_{\epsilon,\bar{\epsilon}}(t,t')G^{\bar{t}}_{\epsilon,\bar{\epsilon}}(t',t)\right],\end{aligned} \tag{15}$$

where indexes t and $\bar{t}$ correspond to time- and anti-time ordering on the Kadanoff-Baym-Keldysh contour, respectively. Then, the corresponding response function (two-particle density of states) in the frequency representation is equal to:

$$\chi_N(\Omega,t_0)=-\frac{1}{\pi}\mathrm{Im}\frac{1}{2\pi}\int dt\int dt' s^2(t)s^2(t')e^{i\Omega(t-t')}R^r(t,t'). \tag{16}$$

We end up with a single-particle contour-ordered Green's function, which we calculate within the DMFT approach. A complete derivation of the DMFT procedure in nonequilibrium has already appeared[16] for the Falicov-Kimball model. We discretize the time interval using three different discretizations Δt and the final result is

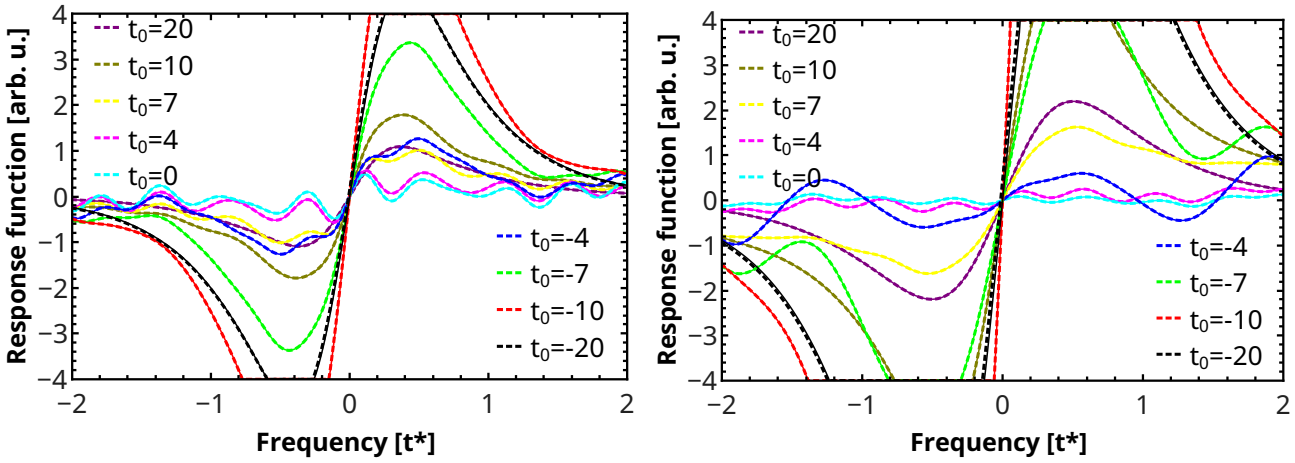

Figure 3. (Color online.) Response functions $\chi_N^{as}(\Omega, t_0)$ (solid line) *vs* $\chi_N(\Omega, t_0)$ (dashed line) for $U = 0.5$ and $T = 0.1$ at different times t_0. The maximum of the pump pulse occurs at time $t_0 = 0$. The left panel corresponds to a wider width of the probe pulse $\sigma_b = 12$, and right panel corresponds to a narrower width of the probe pulse $\sigma_b = 7$. These are the results of the quadratic extrapolation with time discretizations of $\Delta t = 0.066, 0.05, 0.033$. Note that the two possible forms for the response function agree.

found as the Lagrange extrapolation onto the continuous case with $\Delta t \to 0$. Formally, one has to integrate over the time interval from $-\infty$ to $+\infty$ in Eqs. (13, 16), but due to our limited computation resources, we restrict ourselves within a time interval $(t, t') \in [-20, 20]$. This is justified due to the finite extent of the probe envelope functions. To check our results, we verify the spectral moment sum rules which continue to hold in nonequilibrium.[18,19]

3. DISCUSSION

We perform our calculations for the spinless Falicov-Kimball model. This model describes the metal-Mott-insulator transition which occurs at the critical Coulomb interaction $U = \sqrt{2}$. We investigate metallic and Mott-insulator phases along with the critical Mott-insulator. In Figs. 3–5 we present results for the response function $\chi_N(\Omega, t_0)$ obtained from Eq. (14) and Eq. (16) at the initial temperature $T = 0.1$ with different widths of the probe pulse σ_b and at different time-delays t_0 of the probe pulse with respect to the pump pulse. In our calculations, we choose the pump pulse of magnitude $\mathbf{E}_0 = 30$ with a frequency $\omega_p = 0.5$ and a width $\sigma_p = 5$ (to satisfy the sum rules for the discretizations we can calculate, one needs to apply a large pump field[19]).

In Fig. 3, we plot the response function $\chi_N^{as}(\Omega, t_0)$ obtained from Eq. (14) (solid line) and the response function $\chi_N(\Omega, t_0)$ from Eq. (16) (dashed line) for the metallic phase with $U = 0.5$. Different colors correspond to different times t_0 with respect to the pump pulse, whose maximum occurs at $t_0 = 0$. Since all curves obtained from the two different expressions coincide, we conclude that one can continue to calculate the Raman cross-section (correlation function) from the response function (retarded Green's function) for the nonresonant contribution in the B_{1g} channel in nonequilibrium. The magnitude of the response function is significantly suppressed during the pump pulse at times from $t_0 = -4$ to $t_0 = 4$ and its structure is changed from single-peak-like (e.g. around $\Omega = U$ for positive frequencies) to complicated oscillations. At later times, $t_0 = 10, 20$, when the pump is gone, the structure of the response function recovers but the magnitude remains suppressed with respect to the initial one. The width of the probe pulse impacts the response function significantly. The broader probe pulse, with $\sigma_b = 12$ (left panel in Fig. 3), results in a higher energy resolution with many-peaks seen during the pump pulse, while it is much smoother in the case of a narrower probe width $\sigma_b = 7$ (right panel). At the same time, the magnitude of the response function is twice as large for the narrow probe pulse than the broad one.

Similarly, in Fig. 4, we compare the response functions $\chi_N^{as}(\Omega, t_0)$ and $\chi_N(\Omega, t_0)$ for the near critical Mott-insulator phase with $U = 1.5$ (when a gap appears in the equilibrium density of states). Two differences appear

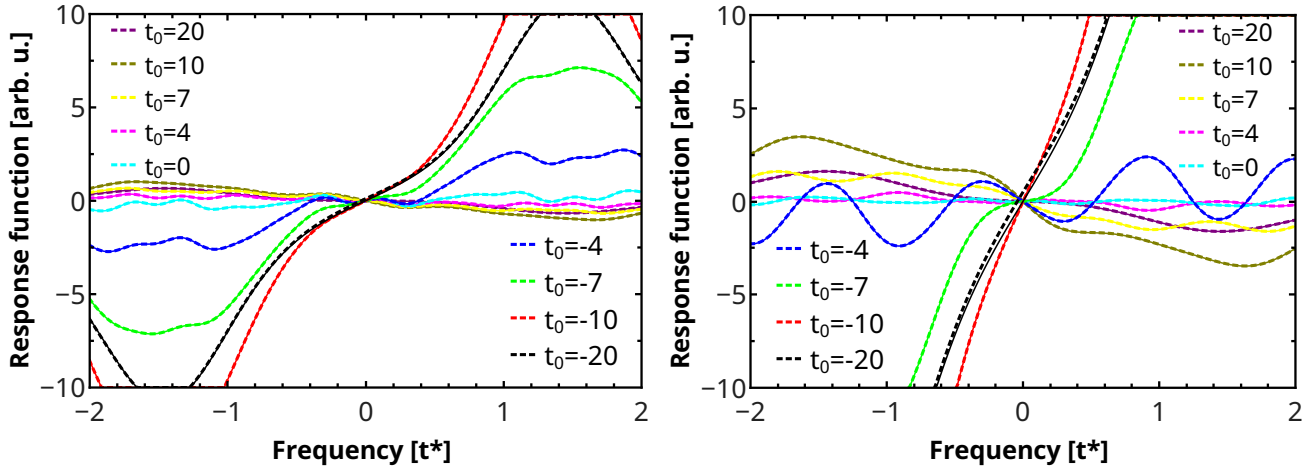

Figure 4. (Color online.) Response functions $\chi_N^{as}(\Omega, t_0)$ (solid line) *vs* $\chi_N(\Omega, t_0)$ (dashed line) for $U = 1.5$ and $T = 0.1$ at different times t_0. The maximum of the pump pulse occurs at the time $t_0 = 0$. The left panel corresponds to a wider width of the probe pulse $\sigma_b = 12$, and the right panel corresponds to a narrower width of the probe pulse $\sigma_b = 7$. These are the results of the quadratic extrapolation with time discretizations of $\Delta t = 0.05, 0.033, 0.025$.

in this case. First, the response function is heavily suppressed by the pump field and becomes almost flat during times from $t_0 = -4$ to $t_0 = 4$. It does not recover even after the pump is gone. Second, the slope of the response function at zero frequency changes its sign at time $t_0 = 0$ (the pump pulse reaches its maximum), and remains even after the pump is gone. This behavior of the response function is specific for this near critical Mott-insulator case.

Finally, in Fig. 5, we present our results for $U = 2.0$, when the system is in the Mott insulating state in equilibrium, with a well developed pseudogap in the density of states of width of $\approx U - 1.5$. In contrast to the previous case of the critical Mott-insulator, the response function demonstrates a complicated oscillating structure for times when the pump field is near its maximum. This complicated structure is seen for both the wide $\sigma_b = 12$ and narrow $\sigma_b = 7$ widths of the probe pulse. The slope of the response function at zero frequency also changes its sign at time $t_0 = 0$, but in contrast to the previous case, it does not remain but changes back to its initial slope at later times, when the pump is gone.

4. CONCLUSIONS

In this work, we described the general formalism for how to solve for the nonresonant Raman scattering in the B_{1g} symmetry channel. For concreteness, we chose to examine the Falicov-Kimball model. We derived analytical expressions for the nonresonant Raman scattering cross-section and the response function. We showed that antisymmetric response functions obtained from two different approaches are equal, which allows us to declare that the connection between the Raman cross-section and the response function holds both in equilibrium and in nonequilibrium. We studied how the nonresonant Raman scattering response function depends on the parameters of the model and of the pump and probe pulses.

ACKNOWLEDGMENTS

This work was supported by the Department of Energy, Office of Basic Energy Sciences, Division of Materials Sciences and Engineering under Contract Nos. DE-AC02-76SF00515 (Stanford/SIMES) and DE-FG02-08ER46542 (Georgetown). Computational resources were provided by the National Energy Research Scientific Computing Center supported by the Department of Energy, Office of Science, under Contract No. DE- AC02-05CH11231. J.K.F. was also supported by the McDevitt bequest at Georgetown.

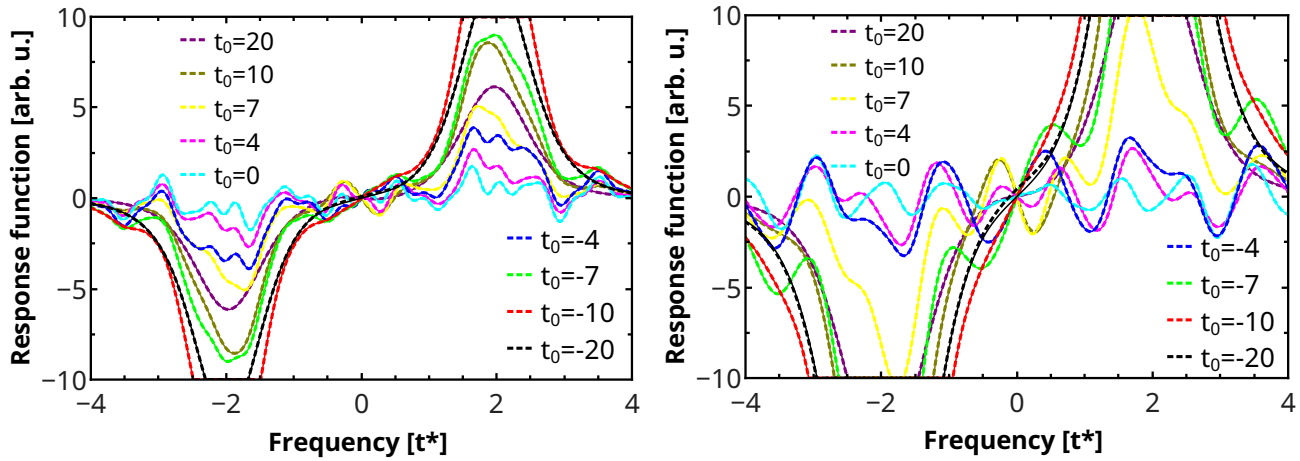

Figure 5. (Color online.) Response functions $\chi_N^{as}(\Omega, t_0)$ (solid line) *vs* $\chi_N(\Omega, t_0)$ (dashed line) for $U = 2.0$ and $T = 0.1$ at different times t_0. Maximum of the pump pulse occurs at time $t_0 = 0$. Left panel corresponds to wider width of the probe pulse $\sigma_b = 12$, and right panel corresponds to narrower width of the probe pulse $\sigma_b = 7$. These are the results of the quadratic extrapolation with time discretizations of $\Delta t = 0.027, 0.022, 0.02$.

REFERENCES

[1] Perfetti, L., Loukakos, P. A., Lisowski, M., Bovensiepen, U., Berger, H., Biermann, S., Cornaglia, P. S., Georges, A., and Wolf, M., "Time evolution of the electronic structure of $1T - TaS_2$ through the insulator-metal transition," *Phys. Rev. Lett.* **97**, 067402 (Aug 2006).

[2] Hellmann, S., Beye, M., Sohrt, C., Rohwer, T., Sorgenfrei, F., Redlin, H., Kalläne, M., Marczynski-Bühlow, M., Hennies, F., Bauer, M., Föhlisch, A., Kipp, L., Wurth, W., and Rossnagel, K., "Ultrafast melting of a charge-density wave in the Mott insulator $1T - TaS_2$," *Phys. Rev. Lett.* **105**, 187401 (Oct 2010).

[3] Hsieh, D., Mahmood, F., Torchinsky, D. H., Cao, G., and Gedik, N., "Observation of a metal-to-insulator transition with both Mott-Hubbard and Slater characteristics in Sr_2IrO_4 from time-resolved photocarrier dynamics," *Phys. Rev. B* **86**, 035128 (Jul 2012).

[4] Wegkamp, D., Herzog, M., Xian, L., Gatti, M., Cudazzo, P., McGahan, C. L., Marvel, R. E., Haglund, R. F., Rubio, A., Wolf, M., and Stähler, J., "Instantaneous band gap collapse in photoexcited monoclinic VO_2 due to photocarrier doping," *Phys. Rev. Lett.* **113**, 216401 (Nov 2014).

[5] Shastry, B. S. and Shraiman, B. I., "Theory of Raman scattering in Mott-Hubbard systems," *Phys. Rev. Lett.* **65**, 1068–1071 (Aug 1990).

[6] Freericks, J. K. and Devereaux, T. P., "Raman scattering through a metal-insulator transition," *Phys. Rev. B* **64**, 125110 (Sep 2001).

[7] Shvaika, A. M., Vorobyov, O., Freericks, J. K., and Devereaux, T. P., "Resonant enhancement of inelastic light scattering in strongly correlated materials," *Phys. Rev. Lett.* **93**, 137402 (Sep 2004).

[8] Shvaika, A. M., Vorobyov, O., Freericks, J. K., and Devereaux, T. P., "Electronic Raman scattering in correlated materials: A treatment of nonresonant, mixed, and resonant scattering using dynamical mean-field theory," *Phys. Rev. B* **71**, 045120 (Jan 2005).

[9] Devereaux, T. P. and Hackl, R., "Inelastic light scattering from correlated electrons," *Rev. Mod. Phys.* **79**, 175–233 (Jan 2007).

[10] Yang, J.-A., Parham, S., Dessau, D., and Reznik, D., "Novel electron-phonon relaxation pathway in graphite revealed by time-resolved Raman scattering and angle-resolved photoemission spectroscopy," *Sci. Rep.* **7**, 40876 (Jan 2017).

[11] Falicov, L. M. and Kimball, J. C., "Simple model for semiconductor-metal transitions: SmB_6 and transition-metal oxides," *Phys. Rev. Lett.* **22**, 997–999 (May 1969).

[12] Brandt, U. and Mielsch, C., "Thermodynamics and correlation functions of the Falicov-Kimball model in large dimensions," *Z. Phys. B: Condens. Matter* **75**, 365–370 (Sep 1989).

[13] Freericks, J. K. and Zlatić, V., "Exact dynamical mean-field theory of the Falicov-Kimball model," *Rev. Mod. Phys.* **75**, 1333–1382 (Oct 2003).

[14] Kadanoff, L. P. and Baym, G., [*Quantum Statistical Mechanics*], W. A. Benjamin, Inc., New York (1962).

[15] Keldysh, L. V., "Diagram technique for nonequilibriun processes," *Sov. Phys. JETP* **20**(4), 1018–1026 (1965).

[16] Freericks, J. K., Turkowski, V. M., and Zlatić, V., "Nonequilibrium dynamical mean-field theory," *Phys. Rev. Lett.* **97**, 266408 (Dec 2006).

[17] Nozières, P. and Abrahams, E., "Threshold singularities of the x-ray Raman scattering in metals," *Phys. Rev. B* **10**, 3099–3112 (Oct 1974).

[18] Turkowski, V. M. and Freericks, J. K., "Spectral moment sum rules for strongly correlated electrons in time-dependent electric fields," *Phys. Rev. B* **73**, 075108 (Feb 2006).

[19] Freericks, J. K., Matveev, O. P., Shvaika, A. M., and Devereaux, T. P., "Theoretical description of pump/probe experiments in nesting induced charge density wave insulators," *Proc. SPIE* **9835, Ultrafast Bandgap Photonics**, 98351F : 1–7 (2016).